Surface Damage Evolution of Graded Materials

M. Besel[1, a], A. Brueckner-Foit[1, b], A. Gruening[1, c], J. Mannel[1, d]

[1]University of Kassel, Institute for Materials Engineering, Moenchebergstr. 3, 34125 Kassel

[a]m.besel@uni-kassel.de, [b]a.brueckner-foit@uni-kassel.de, [c]gruening@uni-kassel.de, [d]j.mannel@uni-kassel.de

Keywords: fatigue, crack initiation, damage parameter, graded material

Abstract. The surface damage evolution of graded materials is investigated within the framework of an ongoing collaborative research center. The first results are presented which deal with the fatigue behavior of engineering steel with an inhomogeneous microstructure. Standard fatigue tests were performed, and the surface damage evolution was observed using an optical long distance microscope. The fatigue test was stopped before failure of the specimen, and SEM pictures of the etched specimen were taken in order to investigate the effect of microstructure on the fatigue behavior. Finally a simple damage parameter is used in order to quantitatively describe the surface damage state.

Introduction

It is well-known that the damage evolution of metals under mechanical fatigue loading consists basically of three stages, namely crack initiation, small crack growth and long crack propagation. While the propagation of long cracks can be described using the concepts of fracture mechanics, it is much more difficult to deal with the phases of crack initiation and small crack propagation because these phases are strongly affected by the material's microstructure [1,2,3]. Analytical models were derived on the basis of dislocation glide, for both crack initiation, e.g. by Tanaka and Mura [4,5], and small crack propagation, e.g. by Navarro and De Los Rios [6]. These models were applied to simulate the crack initiation phase [7,8] as well as the propagation of small cracks [9,10]. These models and simulations focus on specific mechanisms of microstructure changes under fatigue loading. Therefore their application is limited to materials whose damage evolution during fatigue is dominated by one of these mechanisms, e.g. titanium alloys used in aerospace applications [11], or materials with a microstructure designed for specific experimental investigations [10].

This article deals with the fatigue behavior of a low carbon steel in an engineering condition, i.e. a steel with an inhomogeneous microstructure containing a lot of impurities, e.g. carbides and sulphides. Thermo-mechanical forming of round bars results in semifabricated products (flange shafts) with (geometrically) graded material properties due to a graded microstructure as a result of e.g. local martensite transformation [12]. The resulting multiphase structure consists of areas containing ferrite, ferrite/pearlite, and bainite/martensite. The aim of this ongoing research is the characterization of the fatigue behavior of these different microstructures. This paper presents the first results dealing with the surface damage evolution of the raw material, and it is organized as follows. First the raw material's microstructure, and the thermo-mechanically formed semifabricated product with its graded microstructure are presented. Then the experimental procedure is briefly described. Finally the first experimental results are presented showing the surface damage evolution of the raw material. The effect of cementite lamellae on the surface damage evolution is briefly discussed. As a first approximation a simple damage parameter is used to describe the observed surface damage states quantitatively.

Material

The raw material is a CrV-alloyed heat treatable steel (German designation 51CrV4), which is used in typical engineering applications such as shafts, and gears. It is delivered as round bars with a length of 6 m and a diameter of 35 mm in a nominally softening annealed state. Standard tension-tests and hardness tests were performed; the yield strength is about 520 MPa and the Vickers hardness is 244.

Microstructure. Figure 1 shows this typical engineering material with a nearly fully pearlitic microstructure. Various potential crack initiation sites exist, such as carbides or sulphides. The size of the former austenite grains is in the order of 20-100 µm. Murakami etching revealed that most of the carbides are located on the boundaries of the former austenite grains.

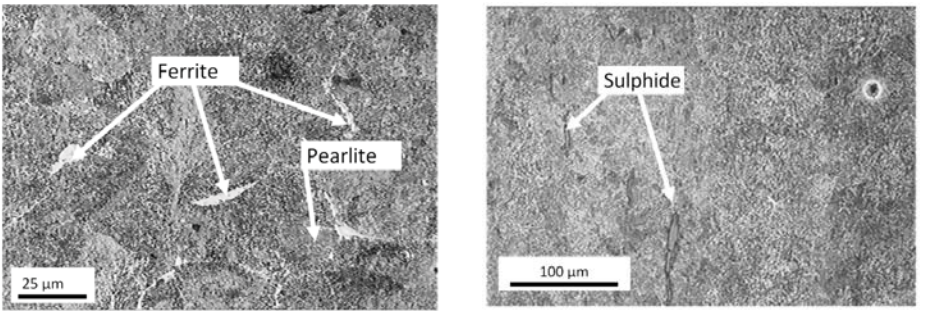

Figure 1: Optical microscope; micrographic etch (2% nitric acid, 6 s) of a cross section normal to the rolling direction

The micrographic etch shows fine-lamellar pearlite areas as well as ferritic areas (network) with a size of several tens of micrometers (see Fig. 1). Comparably hard pearlitic areas are linked by a soft ferrite network. There are sulphide segregations with a width up to 10 µm, and a length up to more than 100 µm. In addition a lot of carbides which may appear as pits on the polished surface were found; the first scan of the polished surface (scanned area about 2.9x3.4 mm²) showed about 48 approximately round black points with diameters in the range of 4-28 µm, and an average diameter of about 11 µm. Cementite appears in different arrangements, such as lamellae, planes, and needles with various lengths, various densities ("number / area"), and various orientations (see Fig 2).

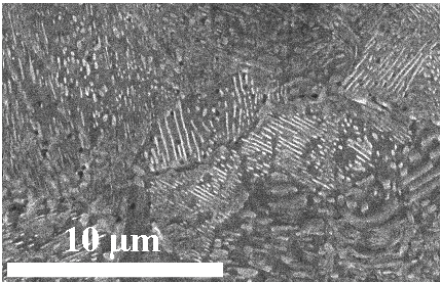

Fig. 2: SEM; cementite and its various arrangements and orientations

The size of the pearlitic areas with the same arrangement of cementite (orientation of lamellae/planes, density) is much smaller than the size of the former austenite grains (see also Fig. 6). Therefore the microstructural length scale affecting the microcracking behavior is even smaller than the 20 µm mentioned above.

Graded material. Thermo-mechanical processing consists of simultaneous forming and heat treatment. The middle part of a round bar (length 200 mm, diameter 30 mm) is inductively heated to about 1300 °C. During the subsequent forming step a flange is formed. The contact cooling due to die-workpiece contact causes local phase transformation; in addition the phase transformation is affected by the local strain during mechanical forming. Details of the thermo-mechanical processing are described elsewhere [12]. Figure 3 shows a micrographic etch of a cross section of the semifabricated product. The different phases, and the geometrical gradient of the microstructure, respectively, can be clearly identified.

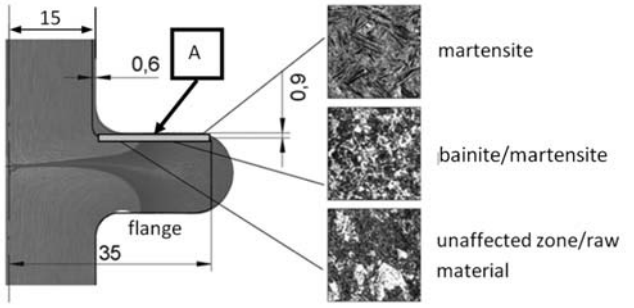

Fig. 3: Micrographic etch of a cross section of the flange shaft

The dark sections in Fig. 3 represent that part of the material bulk that was affected by the thermo-mechanical forming. As a result areas containing bainite/martensite as well as fully martensitic areas exist. The unaffected zone (microstructure of the raw material) appears comparably bright in the overview; its micrograph section shows a microstructure similar to that presented in Figure 1. The residual stresses correlating to the gradient of the microstructure are presented in Figure 4. Residual stress measurements were performed by a standard X-ray diffraction device according to the $\sin^2\Psi$-method, using Cr-K_α-radiation, and the {211}-Bragg peak.

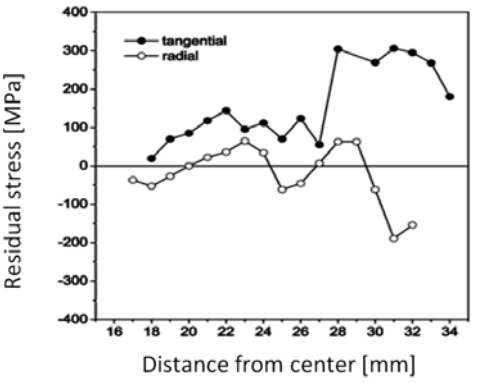

Fig. 4: Residual stresses measured on the top of the flange shaft (see Fig. 3, surface A: striped area)

The raw material in the unaffected zone shows comparably low residual stresses around 0 MPa (tangential and radial; error about ± 15 MPa). The tangential residual stresses rise up to about

300 MPa in the flange, whereas the radial residual stresses oscillate around 0 MPa. This behavior is related to the thermo-mechanical forming process [12]. The thermal influence basically results in a martensitic transformation, and the martensite is subjected to tension residual stresses. The mechanical forming of the flange causes compressive strain and compressive stress, respectively in radial direction, and tension strain in tangential direction. The superposition of the mechanically induced residual stresses with the transformation induced residual stresses results in the residual stress distribution shown in Figure 4.

Judging from Figures 1 to 4 a very complex fatigue behavior of the different microstructure is anticipated. First experiments were performed to investigate the fatigue behavior of the raw material. The experimental setup is described in the next section.

Experimental Setup

Raw Material. Standard fatigue experiments were performed at room temperature with fully reversed loading (R=-1) on a standard servohydraulic testing machine. Symmetrical notched round specimens with a minimum diameter of 6 mm, and a theoretic stress concentration factor of 1.14 are used. The specimens for the S/N-curve were ground; the specimens for the surface observation were ground and polished. The surface observation was carried out with a long distance microscope (Hirox, Japan, working distance 46 mm), that was setup on a computer controlled three-axis stage. The specimen-surface was scanned after a predefined number of load cycles to observe the damage evolution as a function of the number of load cycles. The optical magnification was 750x, and pictures were taken with a 1.14 MPig digital b/w-camera. The scanned surface area was about 2.9x3.4 mm².

The stress level for the surface observation experiment was chosen based on the S/N-curve; the estimated lifetime of the specimen was about 60,000 load cycles. The maximum stress during the fatigue experiment was about 87 % of the yield strength. Each surface scan with the long distance microscope including the corresponding load cycles took about 40-60 min; therefore the stress level was set comparably high to have a feasible experimental time. Although from the macroscopic point of view this seems to be in the transition regime of LCF to HCF, there is no effect on the microscopic level of the damage evolution. In the beginning of the experiment (i.e. mainly crack initiation phase) the surface of the specimen was scanned each 1,000 load cycles, and afterwards the scanning was performed each 2,000 cycles. The experiment was stopped after 18,000 cycles because one crack was found with an apparent length of more than 500 µm, i.e. failure seemed to be imminent. The later detailed observation of the pictures revealed that this crack consisted of three cracks which were nearly coalesced, i.e. at first glance they appeared as one crack. Afterwards some SEM pictures were taken from both, areas of high plastic activity, and microcracks; this step is needed to distinguish surface patterns resulting from plastic activities from those caused by etching of the microstructure. Then the specimen was etched with 2% nitric acid (6 s) to visualize the microstructure. Finally SEM pictures were taken in order to investigate the interaction between the microstructure and the fatigue cracks.

Graded Material. Due to geometrical limitations (see Fig. 3) another type of specimen is needed. Flat and symmetrically notched micro-specimen with a length of about 32 mm and a cross section of about 2.8x2.3 mm² will be used to investigate the surface damage evolution of the different microstructures in the transformed section of the flange shaft.

Experimental Results

Three different sites of crack initiation were identified for the raw material. Crack initiation was found at sulphide inclusions, pits, in the ferrite phase, and at its phase boundaries (ferrite/pearlite), respectively. Figure 5 shows an area of about 0.8x1.3 mm² of the damaged surface after 18,000 load cycles. The polished surface became rough due to local plastic deformation caused by the cyclic loading.

Fig. 5: Extract of the surface scan taken after 18,000 load cycles

The whole surface of the notch (area of stress concentration) is covered with small microcracks and localized plastic deformation, respectively. On the basis of the pictures taken with the optical long distance microscope (Fig. 5) it is difficult to distinguish between microcracks and strong line-like plastic deformation due to the fact that both appear as black lines. But both of them represent an area of locally reduced material strength and therefore contribute to the damage state. As a result in this research work it is not necessary to distinguish clearly between localized line-like plastic deformations (which are becoming cracks) and well defined cracks. This statement can be justified based on Figure 6. Although the etching took only 6 s, and afterwards the specimen was cleaned carefully, new small microcracks appeared immediately after etching in the areas of high plastic activity (see right picture of Fig. 6).

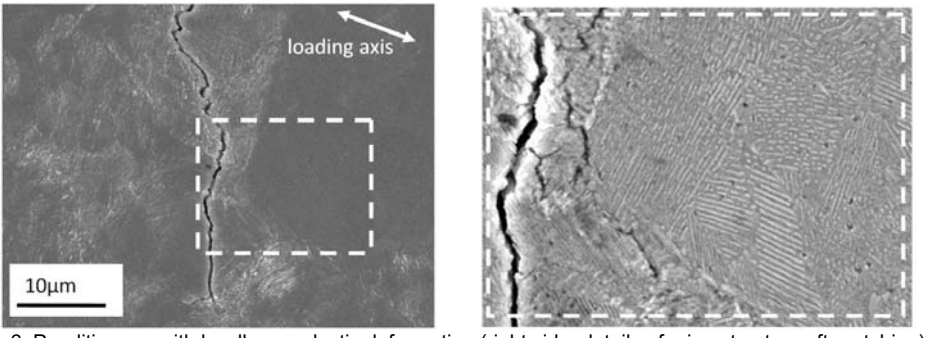

Fig. 6: Pearlitic area with hardly any plastic deformation (right side: details of microstructure after etching)

Figure 6 is representative for the observation, that most of the comparably large areas showing hardly any or no plastic deformation (Fig. 5) correspond to fully pearlitic zones with comparably small spacing between the cementite lamellae (see Fig. 6).

As mentioned above the experiment was stopped because three cracks were found which were about to coalesce, which would result in one crack with a length of more than 500 µm (see Fig. 5, lower right side). At that moment a total of 15 cracks with a length of about 200 µm (or longer) existed on the observed surface. The crack paths of one third (i.e. five) of them were examined in more detail by SEM observations. The effect of the microstructure on the crack propagation is studied by comparison of the SEM pictures (all taken after 18,000 load cycles) with the pictures taken periodically with the long distance microscope. Figure 7 illustrates the procedure.

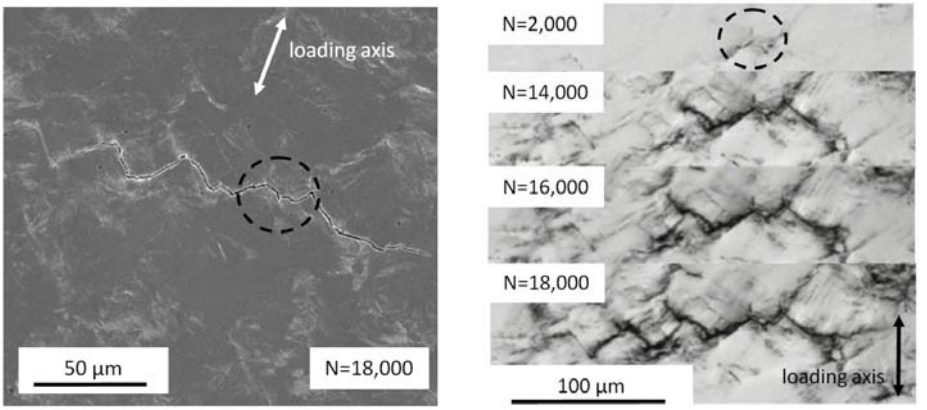

Fig. 7: SEM picture (before etching) and optical microscope pictures showing the same zig-zag crack

The crack shown in Fig. 7 is the only one with this nearly pure zig-zag shape. The orientation of most sections of the crack is either 45 ° or perpendicular to the loading axis. The two dashed circles mark the same section of the zig-zag crack. After 2,000 load cycles a few former pale shades (appeared after 1,000 cycles) became dark lines. These lines propagated during the next applied 1,000 cycles, and therefore either they were already real microcracks after 2,000 cycles, or they became real microcracks within the following load cycles. However, in this paper such lines are treated as microcracks, and with this practical simplification the crack propagation curve of the zig-zag crack is given in Figure 8.

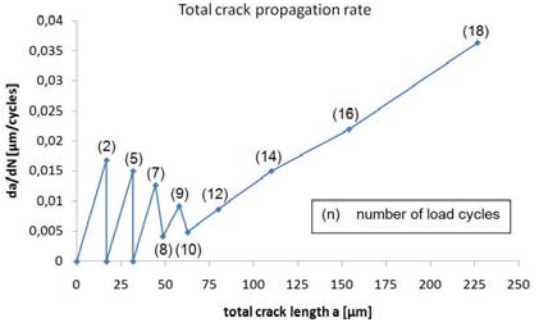

Fig. 8: Total crack propagation rate of zig-zag crack

Figure 8 shows the accumulated crack propagation rate, i.e. the lengths, and the resulting propagation rates, respectively, of all existing sections of the final crack during one scan are summed up. Therefore this diagram of accumulated values represents a kind of averaged crack propagation rate. The typical stop-and-go behaviour of small cracks is observed. The cracks were initiated at grain/phase boundaries (2). Crack stop was caused by pearlite with a comparably high density of cementite lamellae; after changing the direction the cracks continued with intercrystalline propagation. All microcracks (in this case three) coalesced after 7,000 load cycles. The low propagation rate (8) is caused by a pearlitic area with lamellae perpendicular to the crack propagation direction on one side of the crack, i.e. this side is arrested, and the crack propagates only towards the other side. A similar reason is found for the reduced propagation rate at (10); here one side of the crack has to pass through a field of plastic deformed pearlite whose cementite lamellae lay again nearly perpendicular to the crack path. Finally the crack propagation rate increases steadily after the crack has reached a length of about 75 µm. Similar results were found

for the other investigated cracks; the propagation rates of all of them increased steadily after they reached a length of about 75 to 100 µm. It was also found that coalescence of microcracks plays an important role. This is a result of the high crack/line-like damage density (see Fig. 5).

In order to describe the surface damage evolution quantitatively a simple damage parameter is defined based on the statements above concerning the black line-like damages in the pictures taken with the optical microscope. All areas that became darker during the fatigue experiment represent damage, and so they have to contribute to this damage parameter. Therefore the damage evolution is described as the fraction of surface areas that became darker during fatigue; i.e. the dark pixels of each picture are counted [13]. Figure 9 illustrates this idea. The left picture shows a section of the damaged surface taken with the optical long distance microscope. The discussed zig-zag crack is found in the upper middle. All pixels that count for the damage parameter have white color in the right picture. The zig-zag crack can be identified, but in addition the areas of high plastic activity are also included.

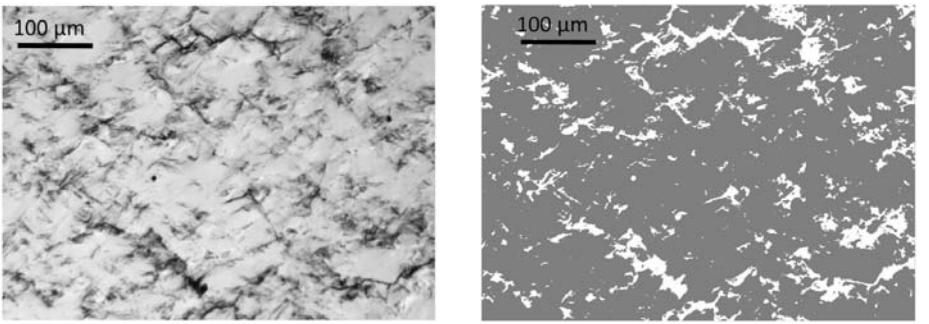

Fig. 9: Damaged surface area (N=18,000) and its contribution to the damage parameter

Figure 10 shows the evolution of the fraction of dark areas during fatigue for the surface area shown in Figure 9. The damage parameter increases monotonously with increasing number of load cycles. The increasing slope indicates the increasing damage evolution of strong plastic activity and initiation and propagation of microcracks, respectively.

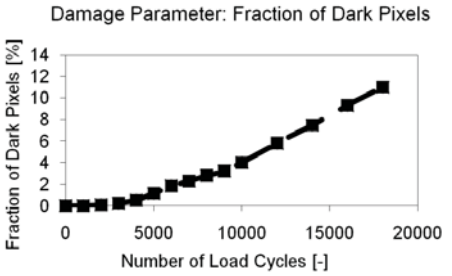

Fig. 10: Damage evolution based on the fraction of dark pixels

The damage parameter is capable to analyse the surface damage evolution quantitatively based on pictures taken with an optical microscope. Real microcracks contribute to this parameter as well as areas of plastic activity. This simple parameter can be used during the crack initiation phase, and the small crack propagation phase, respectively; i.e. it is a useful candidate to evaluate the damage evolution during the fatigue phases which are dominated by the microstructure. It will be used in the ongoing investigations to analyse the complex fatigue behaviour of the different phases in the graded material.

Conclusions

The first results of an ongoing research project dealing with the surface damage evolution of graded steel were presented. Specimens of low carbon steel with an inhomogeneous microstructure (ferrite network, pearlite) were fatigued, and the surface damage evolution was observed with an optical long distance microscope. A complex damage pattern was found. A simple damage parameter was used to evaluate the surface damage state quantitatively. The following conclusions can be drawn.

1. Crack initiation started already during the first 2 % of the estimated lifetime.
2. Most of the cracks are initiated in the soft ferrite phase and at phase boundaries, respectively, and also propagate in these regions.
3. Crack propagation decreased or even stopped in front of pearlitic areas with a high density of cementite; in most cases the crack continues to extend with changing the propagation direction.
4. In this engineering material crack coalescence is an important aspect of small crack propagation; this is due to a high crack density.
5. A simple damage parameter was capable to evaluate the complex damage evolution taking into account both, microcracks, and areas of strong plastic activity.

Acknowledgements

This paper is based on studies carried out by the transregional collaborative research center SFB/TR TRR 30, which is kindly supported by the German Research Foundation (DFG).

Literature

[1] K. Miller, Fatigue Eng. Mater. Struct. 5 (1982), pp. 223-232

[2] M. E. Fine and I. B. Kwon, in: Small Fatigue Cracks, edited by R.O. Ritchie and J. Lankford, The Metallurgical Society (1986)

[3] J. Lankford and D. L. Davidson, in: Small Fatigue Cracks, edited by R.O. Ritchie and J. Lankford, The Metallurgical Society (1986)

[4] K. Tanaka, and T. Mura, ASME J. Appl. Mech. 48 (1981), pp. 97-103

[5] K. Tanaka and T. Mura, Metallurgical Transactions A, Vol. 13A (1982), pp. 117-123

[6] A. Navarro and E. de los Rios in: The behavior of short fatigue cracks, London (1986), European Group of Fracture

[7] X. Huang, A. Brueckner-Foit, M. Besel, Y. Motoyashiki, Engineering Fracture Mechanics, Vol. 74, Issue 18 (2007), Pages 2981-2991

[8] K. S. Chan, Metallurgical and Materials Transactions A, Vol. 34A (2003), pp. 43-57

[9] Y. Akiniwa, K. Tanaka, and H. Kimura, Fatigue Fract Engng Mater Struct, Vol. 24 (2001), pp. 817-829

[10] O. Dueber, B. Kuenkler, U. Krupp, H.-J. Christ, C.-P. Fritzen, International Journal of Fatigue, Vol. 28 (2006), pp. 983–992

[11] Y.M. Hu, W. Floer, U. Krupp, H.-J. Christ, Materials Science and Engineering A278 (2000), pp. 170–180

[12] U. Weidig, K. Huebner and K. Steinhoff, steel research int, Vol. 79, No. 1 (2008), pp. 59-65

[13] M. Besel, A. Brueckner-Foit, Surface damage evolution of engineering steel, Fatigue Fract Engng Mater Struct (2008), submitted 2007